Front Grid Metallization of Silicon Solar Cells

By

Apoorva Srinivasa

A Thesis Presented in Partial Fulfillment

of the Requirements for the Degree

Master of Science

Approved November 2015 by the
Graduate Supervisory Committee:

Stuart Bowden, Chair
William Dauksher
Clarence Tracy

ARIZONA STATE UNIVERSITY

December 2015

ABSTRACT

In order to ensure higher penetration of photovoltaics in the energy market and have an immediate impact in addressing the challenges of energy crisis and climate change, this thesis research focusses on improving the efficiency of the diffused junction silicon solar cells of an already existing line with established processes. Thus, the baseline processes are first made stable and demonstrated as a pilot line at the Solar Power Lab at ASU, to be used as a backbone on which further improvements could be made. Of the several factors that affect the solar cell efficiency, improvement of short circuit current by reduction of the shading losses is chosen to achieve the improvement.

The shading losses are reduced by lowering the finger width of the solar cell .This reduction of the front metal coverage causes an increase in the series resistance, thereby adversely affecting the fill factor and hence efficiency. To overcome this problem, double printing method is explored to be used for front grid metallization. Before its implementation, it is important to accurately understand the effect of reducing the finger width on the series resistance. Hence, series resistance models are modified from the existing generic model and developed to capture the effects of screen-printing. To have minimum power loss in the solar cell, finger spacing is optimized for the front grid design with each of the finger widths chosen, which are narrower than the baseline finger width. A commercial software package called Griddler is used to predict the results of the model developed to capture effects of screen-printing.

The process for double printing with accurate alignment for finger width down to 50um is developed. After designing the screens for optimized front grid, solar cells are fabricated using both single printing and double printing methods and an improvement of efficiency from 17.2% to 17.8%, with peak efficiency of 18% is demonstrated.

DEDICATION

I dedicate this thesis to my outrageously loving and supportive family and also the Almighty. A special feeling of gratitude to my father, Mr. K Srinivasa, for being a constant motivation, for never letting me give up and being my greatest role model, my dearest mother, Mrs. Bhagya Srinivasa, whose selflessness, sacrifice and eternal love has always inspired me to keep going and my sweetest little sister, Anushka Srinivasa, for bringing so much joy and happiness in my life.

ACKNOWLEDGMENT

I wish to express sincere gratitude to my advisor, Dr. Stuart Bowden, for giving me the wonderful opportunity to do research work at the Solar Power Laboratory (SPL) at Arizona State University (ASU), for having a lot of faith in me, for constant support and invaluable guidance. I would like to express a special word of thanks to Dr. Christiana Honsberg for believing in my capability, and being an inspiring role model in the world of solar and photovoltaics and women in science everywhere. I would like to thank the lab maestro of SPL, Bill Dauksher, for showing infinite reserves of patience during the entire research and for being more than generous with his expertise and precious time. I also wish to express my sincere thanks to Dr. Clarence Tracy for teaching invaluable concepts of solar cells, always answering all my incessant questions with a very calm demeanor and encouraging smile. I am grateful to all of them for providing me with invaluable insights and pushing me to expand the horizons of my knowledge.

Furthermore, I would like to extend my appreciation to Stanislau Herasimenka and Joseph Karas for their patience and help throughout my research and providing valuable feedback.

Finally I would like to express my loving thanks to all my fellow PV engineers of Silicon group at SPL, for being a great support throughout, offering me words of encouragement when I needed it the most, and for making this great learning experience so much fun.

TABLE OF CONTENTS

Page

CHAPTER Page

LIST OF TABLES

Table Page

LIST OF FIGURES

Figure Page

Figure Page

Figure Page

1. INTRODUCTION

Combating energy crisis and climate change are arguably two of the biggest challenges the world will have to face in the coming century. Our energy infrastructure is currently heavily based on the combustion of fossil fuels. The potential impacts of continued usage of the fossil fuels to meet the ever increasing energy demands associated with increase in population and increase in per capita energy consumption could be catastrophic on the environment and also lead to the depletion of the limited reserves of fossil fuels in the world. This challenge exists in industrialized and developing countries alike. Thus there is an urgent need for a profound transformation in our energy infrastructure to one that is cleaner, renewable, efficient, carbon free and an environment friendly. One of the best ways of doing this is to meet our increasing energy demand curve with new renewable resources, rather than new traditional ones [1]. Development and deployment of renewable energy technologies needs to be accelerated in an environmentally responsible and sustainable way [2].

Renewable energy contributes to economic growth, energy independence, and carbon mitigation. To achieve high levels of renewable penetration in the future and promote utilization of renewable energy, more work is needed to continue lowering the cost of renewable energy technologies, while increasing their reliability, expanding transmission, and improving grid integration. Fortunately, in recent years, progress has been made in developing cleaner, more efficient energy technologies. The use of low-carbon energy sources is expanding rapidly, and there are signs that growth in the global economy and energy-related emissions may be starting to decouple. Renewable technologies are becoming increasingly cost competitive in a number of countries and circumstances, but public support schemes are still required to support deployment in

many others. [3]. More than 50% of global power investments are in clean energy systems, and the renewables industry continues to grow around the world [4] as illustrated by figure 1. The installed global renewable electricity capacity more than doubled between 2000 and 2013, and comprises 27% of the total electricity capacity globally, representing a significant and growing portion of the total energy supply [3].

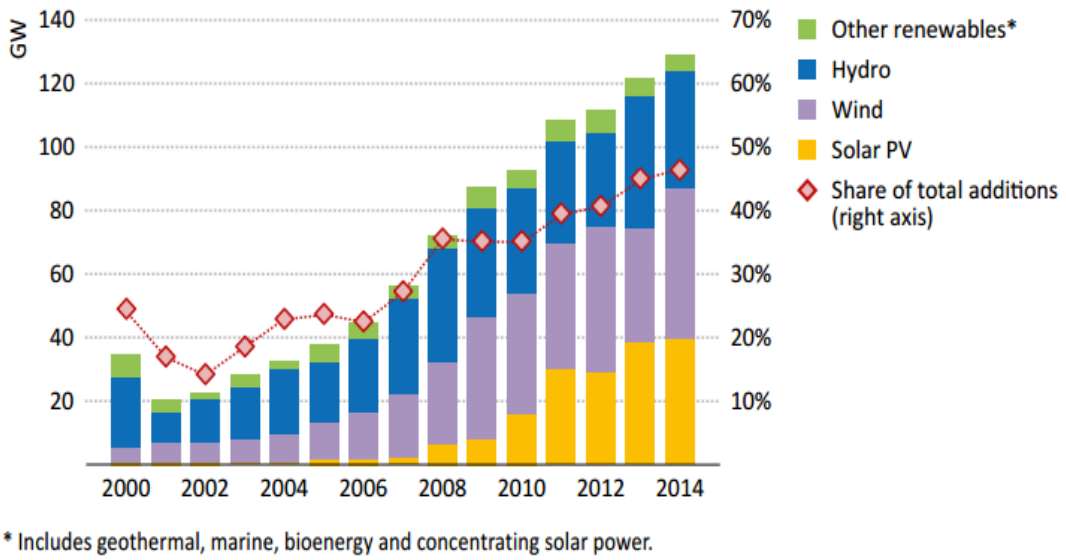

Figure 1: Global Renewables-based Power Capacity Additions by Type and Share of Total Capacity Additions [3]

Photovoltaics is one of the emerging technologies for alternate sources of energy that has the potential to simultaneously address the climate-change and energy-security concerns. It can prove be a great solution to the increasing needs for clean energy source because of the unlimited energy provided by the sun if harnessed efficiently. Harnessing solar energy has various advantages since it's non-polluting, clean, and abundantly available throughout the year, indefinitely renewable source of energy and it presents us

with the opportunity to power a village or a home which is not even connected to an electrical grid powered by utility-scale power plants.

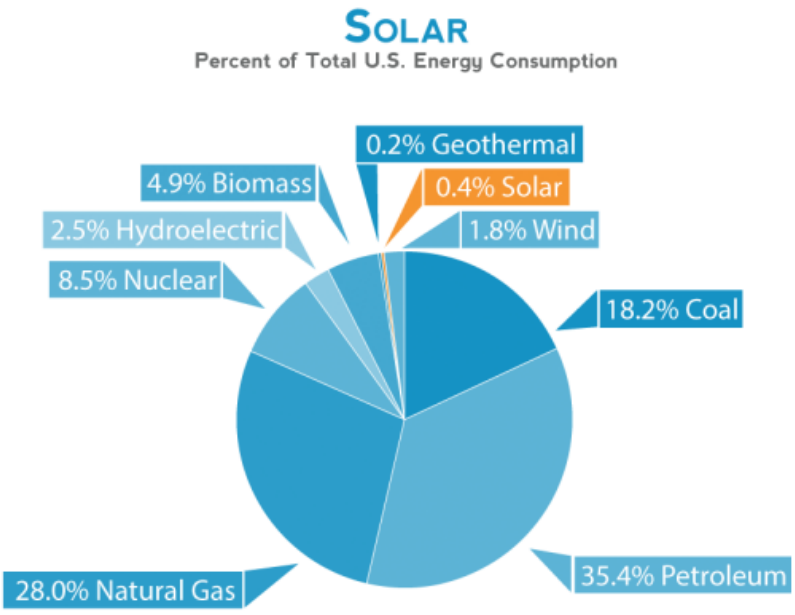

Figure 2: Contribution of Solar Energy as a Percent of Total US Energy Consumption [5]

It is seen from figure 2 that even though steadily increasing, the total share of solar energy in the energy market is still very low. Figure 3 shows the dramatic decline of PV price over the years. The three most important factors that have been influential in bringing about this change are the size and scale of the fabrication plants, the efficiency of the solar technology to convert sunlight into electricity, and the cost of the primary resource in the majority of these modules – silicon [6]. Silicon wafer based PV technology constitutes for almost 90% of the total market share. According to analysts, the pricing in all PV markets will continue to decrease in the long term [7] as shown in the figure 4.

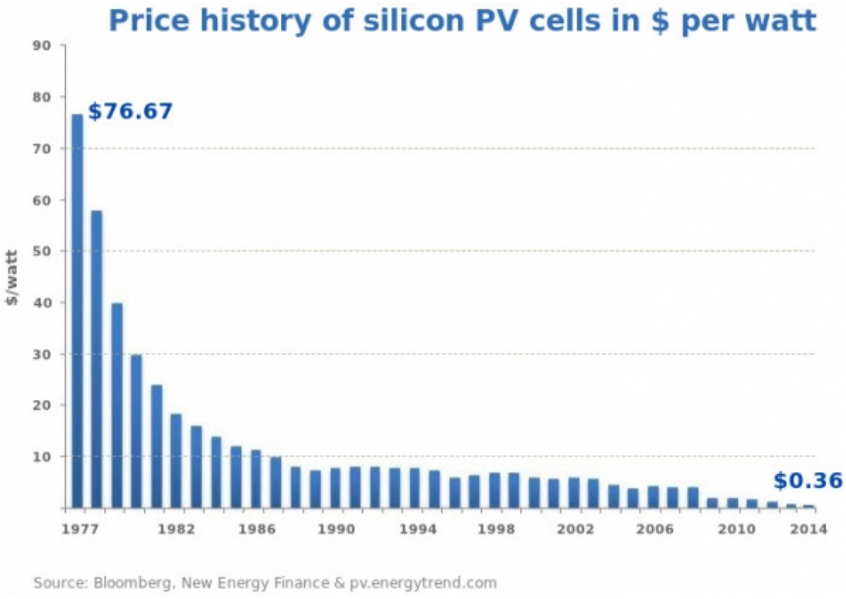

Figure 3: Historical Decrease in Price of PV Cells in $ per Watt [8]

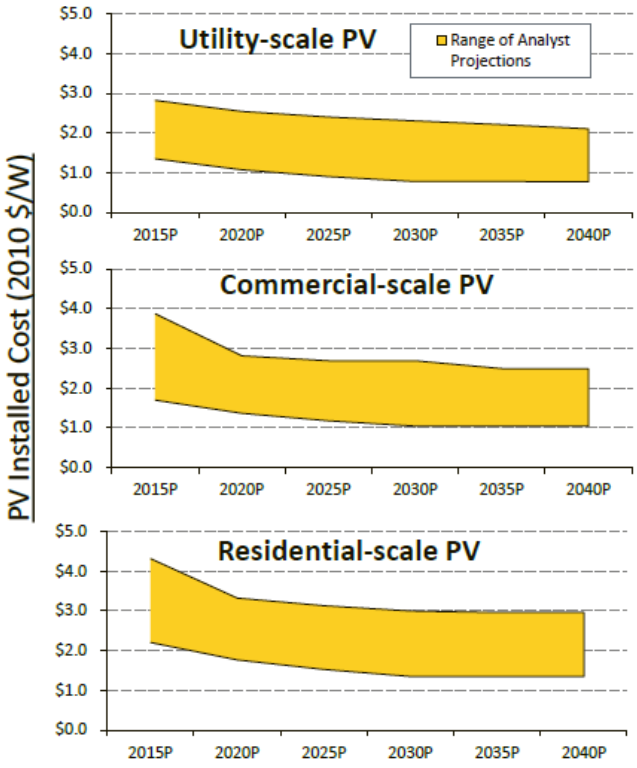

Figure 4: Range of Analyst Expectations of Long-term System Price [7]

2. MOTIVATION

To ensure more and more penetration of PV in the market, it is imperative that the trend of falling prices of PV continues. One of the effective ways of doing that could be by optimizing the front grid metallization. By doing so it is possible to improve the efficiency of solar cells. Improving the conversion efficiency will lead to higher power output of solar cells. And this increase in conversion efficiency will result in lowering of the overall cost as more watts can be obtained from lesser number of solar cells or modules [9]. Due to this, in addition to saving cost on balance of system and cost of labor, less land area would be required to install more capacity (in terms of watts) which could lead to substantial cost savings.

Optimizing the front grid design and then using the double printing method or stencil printing, which will be discussed later in detail, has the potential to reduce the silver paste consumption [10, 11, 12]. Silver is the preferred metal for front side metallization as it has the lowest electrical resistivity of all the pure metals [13]. It is used as a contacting agent between the wafer and the finger line and conduct the generated current in the solar cells. The standard silver based paste is composed of silver powder along with inorganic glass and other additives suspended in a solvent. Silver is an expensive metal. The price of photovoltaics depends on the silver metallization cost as it accounts for roughly around 30% of the total cost of the cell [14]. Thus, for the price of PV to continue to fall there has to be reduction of silver usage without sacrificing cell efficiency [15].

The driving factor behind the work at Solar Power Laboratory presented in this thesis was the expansion of lab capability through the addition of Semi-automatic

Baccini printer (figure 5) to the tools and equipment in the lab. The double print method to print contact lines on the solar cells require very high alignment accuracy for good print results and high degree of repeatability; the second print layer must be perfectly placed above the first. Applied Baccini's Semi-automatic screen-printer has exceptional alignment and fine-line capabilities. It utilizes multiple high resolution cameras, illumination systems and software algorithms to provide superior alignment accuracy. Thus, it was a great opportunity to make use of this tool as a backbone and introduce double printing in the work of optimizing the metallization at the Solar Power Laboratory.

Figure 5: Baccini Semi- Automatic Lab Printer at SPL

3. DIFFUSED JUNCTION SOLAR CELL PILOT LINE AT SPL

Presently, the most popular solar cells on the market are the crystalline silicon PV cells. Of all types of commercial solar cells, besides having the advantage of a long history of proven operation on the field, they provide the highest efficiencies while presenting fewer resource issues as compared to many competing technologies. So crystalline silicon PV cells are expected to keep being well represented even in the future market [16]. To ensure continued growth in the market it is necessary to develop new tools and processes so that manufacturing remains efficient and cost effective. For the development and transfer of new materials and processes to industry, there needs to be a pilot line in R&D labs that is relevant and compatible with the majority of the industry from market point of view. This will enable optimization of each step in the process flow to get the best results. The parameters affecting each step can be studied and changed accordingly to improve the overall cell. The effects of these changes can be studied and once the process flow with the change is stabilized, next step can be optimized and so on. This allows for continuous mass production of solar cells, at the same time allowing implementation and incorporation of new processes and testing into the process flow without affecting the existing ones.

It is with this idea the student-led diffused junction solar cell pilot line at ASU Solar Power Laboratory was established. It is a unique facility in which undergraduate students, graduate students, researchers, and industry fabricate and characterize silicon solar cells and modules. A pilot line is also an effective means to train personnel and future PV engineers for a full-scale plant.

The endeavor to have an established student-led pilot line for Heterojunction structured silicon solar cell has become successful. However, this thesis will focus only on the diffused junction p-type base solar cell pilot line. Figure 6 depicts the cross section of a standard diffused junction solar cell.

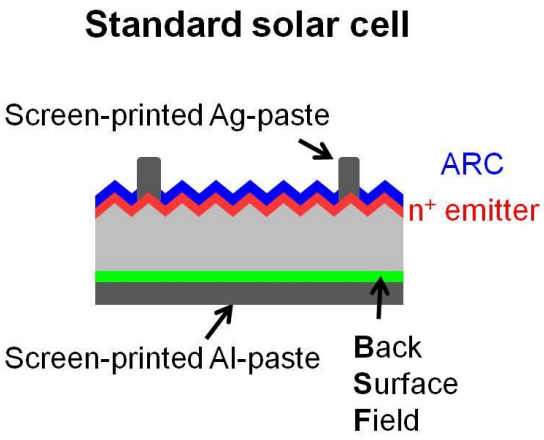

Figure 6: Schematic Drawing of a Standard Diffused Junction Si Solar Cell [17]

The process flow and the steps followed are as follows:

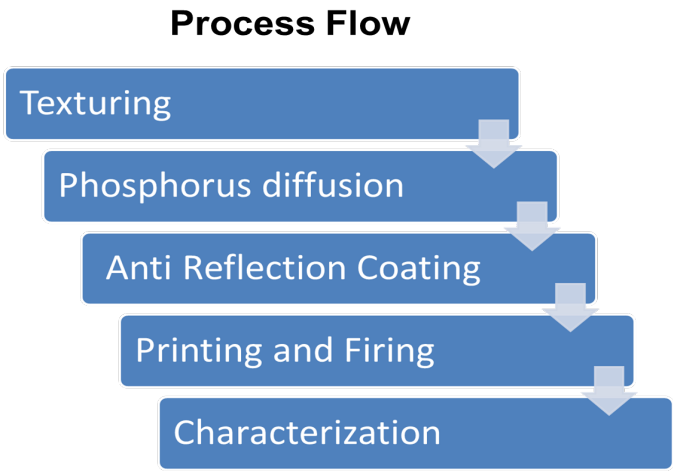

Figure 7: Process Flow for the Diffused Junction Solar Cell Pilot Line

3.1 Texturing

The p-doped monocrystalline wafers obtained from the vendor are dipped into the potassium hydroxide solution to get rid of the micro cracks and saw damage on the surface. They are then dipped into a different potassium hydroxide (KOH) solutions with substantially lower concentration for anisotropic selective chemical etching of the <100> Si surface which results in the formation of small random pyramid structures [18] as seen in figure 8. This helps in reducing the reflection of light from the surface of the cell, thereby, increasing the absorption of light into the cell [19]. After texturing, the wafers at SPL typically have reflectivity around 10.0-10.4% at 700 nm as shown in the figure 9.

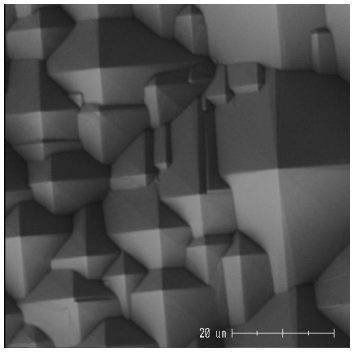

Figure 8: SEM Image of Si Textured in KOH Solution at SPL [20]

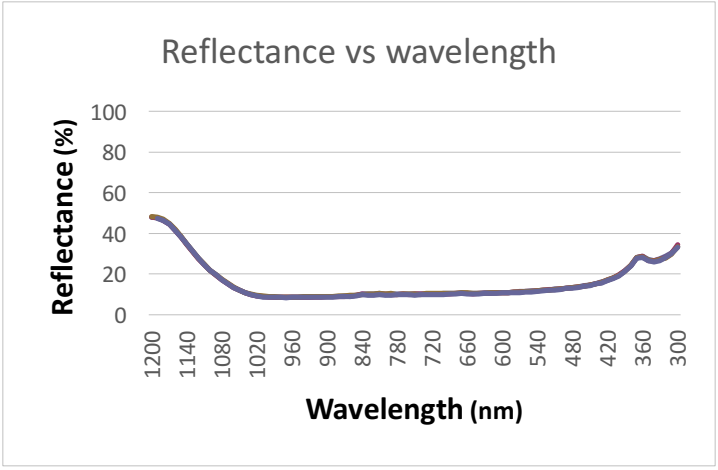

Figure 9: Graph of Reflectance vs. Wavelength of a Textured Cell at SPL

3.2 Diffusion

Before diffusion is performed on the baseline cells, a thick layer of silicon dioxide (2000 Å) is deposited in the PECVD tool at the back of the wafer so as to get a n-type emitter after diffusion only on one side (on the front side) of the wafer.

Phosphorous (P) diffusion to form the n-type emitter on the p-doped wafer is arguably the most crucial step in the fabrication of silicon (Si) solar cells as it is this process that converts a wafer into a P-N junction device. The emitter formation is realized by using phosphorous-oxychloride ($POCl_3$). For uniformity and better quality, the wafers placed side-by-side horizontally in quartz boat are placed on a cantilever beam and the diffusion occurs in a $POCl_3$ tube. Temperature, gas flow rates and their composition are some of the important conditions that have an impact on the emitter properties [21].

The following are the primary steps in diffusion using $POCL_3$:

1) Pre-depostion: Initial pre-dep step precedes doping. This step introduces the required amount of dopant into the substrate and forms PSG.
2) Drive in: The dopant is then redistributed, and P from the PSG diffuses into the Si substrate in this drive-in anneal step, the giving the required junction depth and surface concentration.

A typical cell following the baseline diffusion recipe has ECV profile (a phosphorus concentration vs depth profile as measured by electrochemical capacitance voltage) that looks as shown in the figure 10 below:

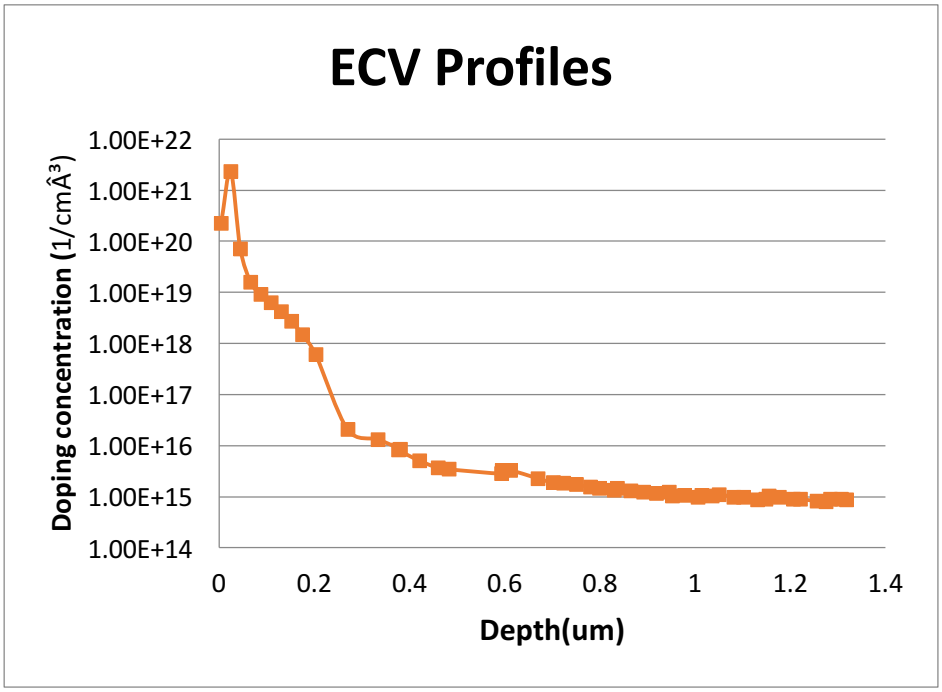

Figure 10: ECV Profile of a Diffused Junction Solar Cell Produced in SPL

Then, the Phosphosilicate glass (PSG) on the diffused wafers created during diffusion is etched off in a hydrofluoric acid solution.

3.3 Anti Reflection Coating

Even though texturing reduces the reflection of light from the surface of the cell, to further reduce the reflection of incoming radiation from sun in order to maximize the absorption of light, a silicon nitride film (SiN_x), which acts as Anti reflection coating (ARC), is deposited by plasma enhanced chemical vapor deposition (PECVD) on the front surface of the solar cell. The silicon nitride film serves as a passivating layer for the front surface of the solar cell in addition to serving as an anti-reflection coating. Thus, it is important that the film must be optimized to absorb the majority of incoming radiation as well as passivate the surface satisfactorily. The target thickness of ARC for baseline cells is set at 780nm.

Figure 11: A Silicon Nitride Coated Cell

3.4 Printing and Firing

3.4.1 Backside Printing

Aluminum is used to form the back contact of the cell. The full-coverage aluminum back contact also acts as a passivating layer. Aluminum is a group III element, thus acting as a p-type dopant in silicon. The p^+-p junction caused by higher doping of the back surface due to the layer of aluminum on the p-doped substrate leads to the formation of a back surface field (BSF) which can reduce the surface recombination at the back surface [22]. The backside printing of Al-BSF of the cells at SPL is done in MPM printer which is shown in figure 12. The cells are then dried in drying furnace before printing the silver front grid on them.

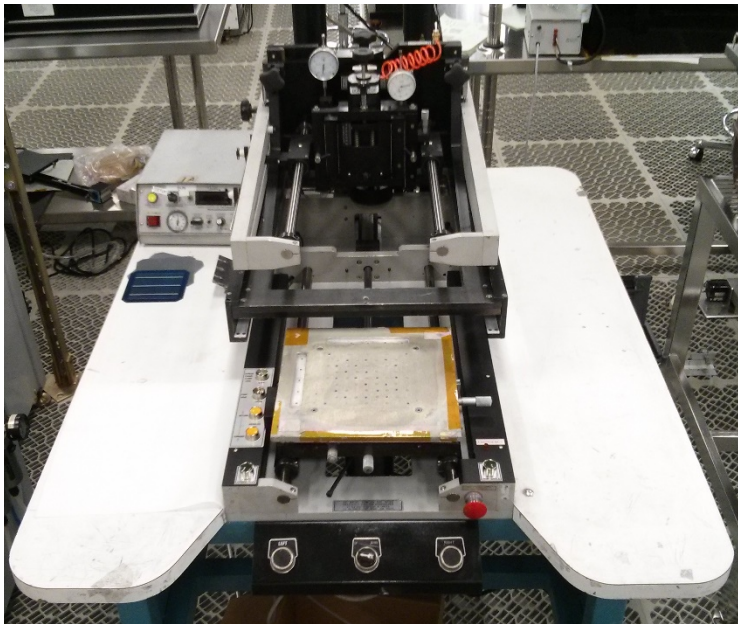

Figure 12: MPM Printer at SPL for Printing Al-BSF

3.4.2 Front Grid Printing

Screen-printing of the metal contacts using the silver paste onto the front side of solar cells results in printing of 90um wide fingers and 1.5mm wide busbars to collect and carry the current generated. The AMI MSP-9156PC semi-automatic screen-printer is used to deposit Heraeus SOL9610Y paste with the help of mesh screen fabricated by Photo Stencil. After front grid printing, cells are again dried in the drying furnace before being co-fired (firing recipe used is CXT0435I) to form contacts.

3.5 Characterization

Precisely determining the output data of photovoltaic components using various types of measurement methods is important to analyze the performance of the solar cell manufactured. At SPL, mainly three types of characterization tools are used:

IV Tester: Sinton FCT 400 for measuring the output conversion efficiency, open circuit voltage (Voc), short circuit current density (Jsc), fill factor (FF), series resistance (Rs) and shunt resistance (Rsh) of the cell

QE Tester: The "quantum efficiency" (Q.E.) is the ratio of the number of carriers collected by the solar cell to the number of photons of a given energy incident on the solar cell. The "external" quantum efficiency of a silicon solar cell is measured using the QEX10 measurement tool from PVMeasurements Inc. which shows the effect of optical losses such as transmission and reflection [23].

EL/PL tool: Electroluminescence is an effective way to analyze the poorly contacted and, inactive and recombination dominant regions of solar cells as these regions show up as dark areas in the EL image as seen in figure 13. It is helpful in detecting problems like micro cracks and printing problems which cannot be detected by visually looking at the solar cells.

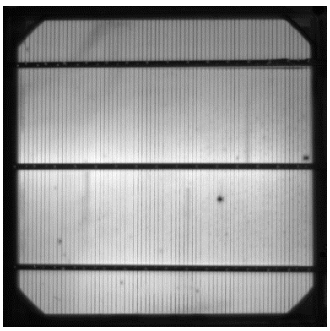

Figure 13: Electroluminescence Image of a Pilot Line Cell at SPL

3.6 Pilot Line Goals

Various optimization experiments are run from time to time when any drift in parameters is observed due to changes in supply of pastes and chemicals or drift due to changes in tool properties or settings. Experiments are also run to improve the processes in order to achieve higher conversion efficiency of the baseline solar cells.

The goal of the pilot line is two-fold:

1) To have a repeatable, stable and controllable set of baseline processes to make standard diffused junction solar cells.
2) To continually push the baseline towards higher efficiency.

Currently, the baseline solar cells have the following output parameters:

Table 1: Output Parameters of Diffused Junction Baseline Cells at SPL

Parameters	Values
Efficiency	17.2%
Voc	616 mV
Jsc	35.5 mA/cm2
FF	78.8%

In this thesis, these values will be used as a reference to compare the performance of cells with optimized metallization of the front grid.

4. LOSS MECHANISMS

The maximum theoretical limit of conversion efficiency for a single-junction crystalline silicon solar cell under one sun is approximately 29% [24, 25]. However, owing to different types of loss mechanisms, the solar cells practically have much lower efficiencies compared to this theoretical number. It is important to analyze and understand the various loss mechanisms in order to identify the certain efficiency restrictions.

There are some inherent loss mechanisms in the solar cell which cannot be totally avoided or reduced beyond a certain limit because of their fundamental nature. As explained in [26], following are the losses fundamental losses:

1) Loss due to low energy of photons: The photons that have energy less than the energy of the bandgap of the material (E_G) cannot be absorbed and so can't generate any electron-hole pairs.
2) Loss due to excess energy of photons: The photons that have energy more than the energy of the bandgap of the material give off the excess energy ($E- E_G$) in the form of heat.
3) Voltage loss: The maximum voltage obtained from the cell is the open circuit voltage (Voc), is less than the bandgap voltage for a given material (the voltage corresponding to the bandgap of the material obtained by dividing E_G by the charge, i.e. Eg/q) because of unavoidable intrinsic Auger recombination.
4) Fill factor loss: The exponential behavior of the IV curve of the cell deviates from the square shape of the ideal solar cell which would have FF=1. This happens because of the parasitic resistances of the cell.

There are other losses, due to constraints in solar cell processing capabilities, called technological losses. They can be broadly categorized as optical losses and electrical losses.

Optical losses result in the reduction of photon absorption, which, if absorbed, would have generated electron hole pairs.

1) Reflection loss: Loss due to the reflection of the light incident at the front surface.
2) Shading loss: Loss due to the coverage of front surface with the contact metal.
3) Transmission loss: Loss due to the escape of photons from the cell (incomplete absorption) due to the limited solar cell thickness.

Electrical losses are due to the photons which are absorbed in the cell but fail to contribute to the output power of the cell.

1) Resistive loss: Loss due to series and shunt resistance of the solar cell.
2) Recombination loss: Loss because of the photo generated electrons and holes that recombine in the bulk or surface of the cell before being collected at the cell contacts.

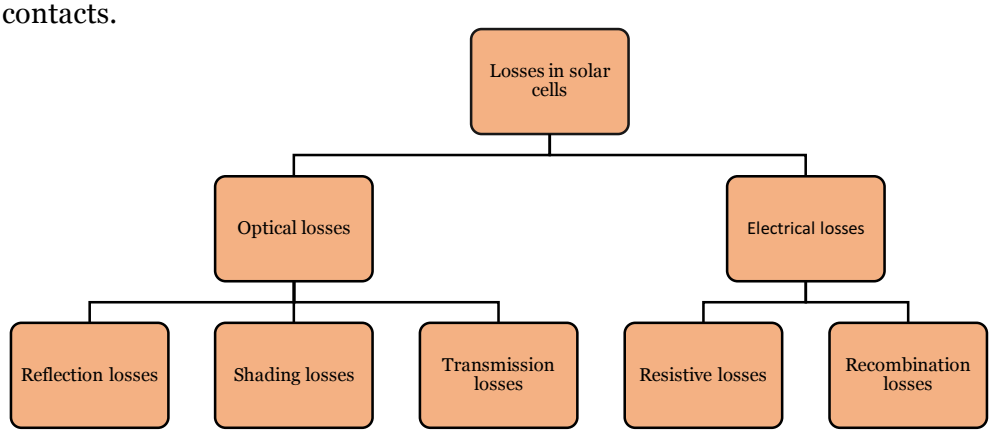

Figure 14: Loss Mechanisms in a Solar Cell

5. MAXIMIZING EFFICIENCY

The efficiency of a solar cell is the fraction of input energy from the sunlight that is converted into output as electrical energy. The efficiency formula [27] is given by:

$$\text{Efficiency, } \eta = \frac{V_{oc} I_{sc} FF}{P_{in}} \quad 5.1$$

Where,
V_{oc} is the open-circuit voltage;
I_{sc} is the short-circuit current;
FF is the fill factor;
and η is the efficiency.

To facilitate comparison of the performance of one terrestrial solar cell to another, for efficiency calculations, measurements are done under set standard conditions of AM 1.5 spectrum and temperature of 25°C with input power density as 1 kW/m² or 100mW/cm².

Thus, it is seen that, the efficiency of the solar cell depends on (and is directly proportional to) the short circuit current (Isc) of the cell. In this thesis, the approach taken towards increasing efficiency of the baseline cells is by focusing on improving the short circuit current (Isc) of the cell. There are different factors which affect the Isc of the cell, hence, there are different methods which could potentially improve the Isc of the cell. Out of those, this thesis deals specifically with reducing the shading losses to increase the incident light on the surface and achieve the desired improvement in short circuit current (Isc) in order to improve efficiency of the cell.

Shading, due to the front coverage of metal for contact, reduces the front active area of the cell and thus limits the short circuit current. According to the simulated

results for a conventional homogenous phosphorus doped emitter solar cell in [28], the area losses (shading losses) contribute to around 17% of the total losses as depicted in the figure 15.

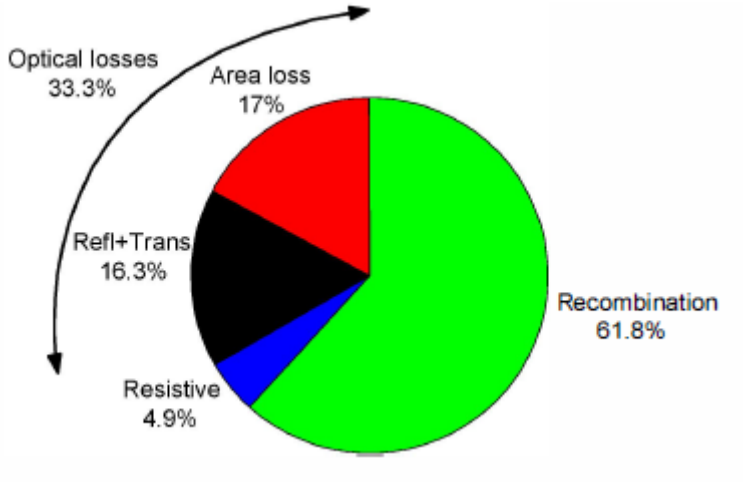

Figure 15: Pie Chart of the Contributions of Various Losses in the Diffused Junction Solar Cell [28]

Shading losses can be reduced by reducing the finger width or number of busbars (which reduce the cross-sectional area) of the front contacts, but this might lead to an increase in series resistance as evident from the following basic equation of resistance in which the width '*w*' is inversely proportional to the resistance '*R*':

$$\text{Resistance, } R = \frac{\rho l}{A} = \frac{\rho l}{wt} \qquad 5.2$$

Where ρ is specific resistivity of the material, *l* is the length, w is the width and *t* is the thickness of the given conducting medium of the given material.

6. SCREEN-PRINTING

6.1 Overview

There are many technologies for metallization like screen-printing, inkjet printing, pad printing, dispensing, laser micro-sintering, photolithographical and evaporation process and plating. Screen-printing still remains as the most commonly used technology for solar cell front and rear side metallization in the industry. Many reasons contribute to this, like relatively simple and fast method, high throughput rates, reliability and reduced cost as compared to other printing methods [29]. However, in our endeavor towards reducing the finger width so that shading loss can be reduced and short circuit density can be improved, the series resistance inherently increases, thereby negatively affecting the efficiency of the solar cell because of the reduced fill factor. In order to incorporate all the benefits of the screen-printing technology and at the same time reduce the unwanted effect of increase in series resistance as much as possible, it is important to investigate an advanced screen-printing method. 'Pattern-on-pattern' method of screen-printing could be the solution to the aforementioned problem, which will be discussed in the subsequent section of the chapter.

6.2 Double Printing

The term double printing is a generic term that can be used to describe any printing process that applies two consecutive screen-printing steps. The two different double printing methods investigated by the industry and R&D institutions are: Dual printing and Print-on-Print method. Both the methods have their own set of advantages and require high alignment accuracy to carry out the two steps.

The method used for this thesis work primarily is Print-on-Print, thus, henceforth the term double print will refer to the print-on-print method (or pattern-on-pattern printing), unless specified otherwise.

6.2.1 Dual Printing

In dual printing, only the busbars are first printed on the cell using a mesh screen, after which the cell is then dried. It is assumed that after drying, the wet print would become fairly stable so the second print over the first one wouldn't cause over broadening of the fingers [30]. In the second step, the fingers are printed using a stencil screen to get the final full pattern (shown in figure 16), which is dried again and finally fired. This method will not be explained in detail as it will not be applied in the work done for this thesis.

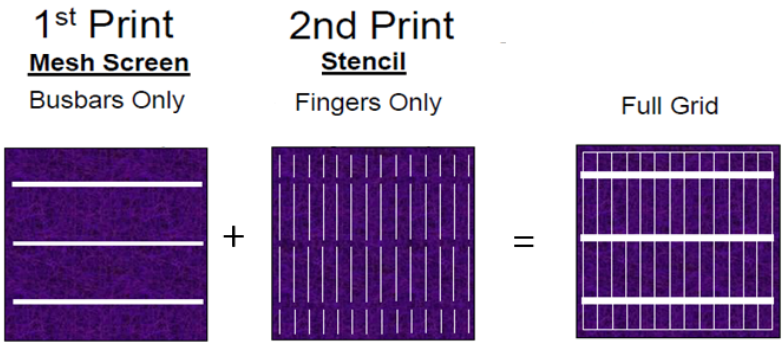

Figure 16: Representation of the Printing Steps for Dual Print Method [31]

6.2.2 Print-on-Print

Print-on-print or Pattern-on-pattern printing (PoP) is the method which consists of two consecutive mesh screen-printing steps, in the first step only the fingers are printed and a second layer of paste is printed over the first with the full grid pattern (as

shown in figure 17). Like in dual print process, the cell is dried after before and after the second print step and finally fired. The schematic of the final solar cell is as shown in figure 18.

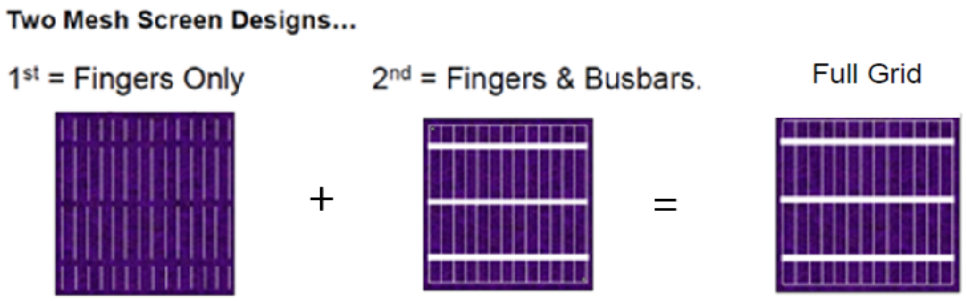

Figure 17: Representation of the Printing Steps for Print-on-Print Method [31]

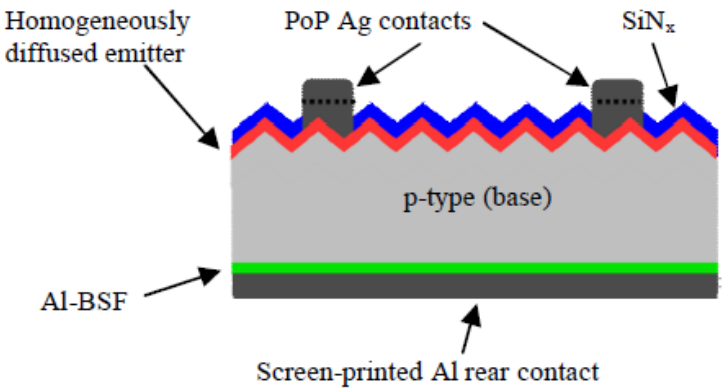

Figure 18: Schematic Drawing of the Industrial Type Silicon Solar Cell with Print-on-Print Ag Front Contacts [32]

Depending on the pastes used for the two consecutive printing steps, the print-on-print method can be categorized as generation I and generation II concepts for the double printing [33]:

- The generation I concept uses the same paste for both the first and the second printing step. This gives better aspect ratio as the height of the fingers is increased due to two prints.
- The generation II concept uses different pastes for 1st and 2nd prints: The first paste optimized for contacting the emitter layer and the second paste containing less frit and more Ag content, optimized for better conductivity [33]. The second paste, apart from being optimized for better conductivity, should preferably be non-firing through, so that the busbars (which are printed in second print) aren't fired through the SiN_x, thus not making contact with the emitter. These can also be called as "floating bus bars" [34].

Double printing (DP) has several advantages over single printing (SP). Some of them are as follows [10-12, 30-33]:

- Higher aspect ratio of the fingers (illustrated in (b) of figure 19)
- Less shading and hence more active area on the front
- Improvement in Jsc and thus, efficiency
- Reduced paste consumption
- Overall cost saving (due to above factors)

And, by the virtue of differentiated pastes for the two layers (in case of DP generation II),

- Better current carrying capability
- Reduction of recombination under the busbars due to floating busbars resulting in higher Voc

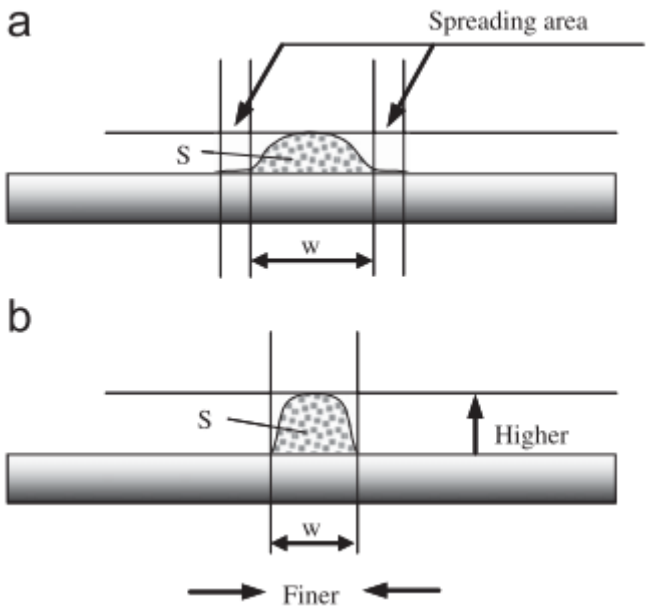

Figure 19: Illustrative Diagram of Cell with (a) Lower and (b) Higher Aspect Ratio [35]

To understand and accurately study the effect of reducing the area of front metal coverage, it is important to model the series resistance of the solar cell as an increase in series resistance of the cell will lead to a reduction in fill factor (FF), which might adversely affect the efficiency. The following chapter deals with the modelling of series resistance of solar cells

7. LOW LOSS METALLIZATION PATTERN

7.1 Modelling of Series Resistance

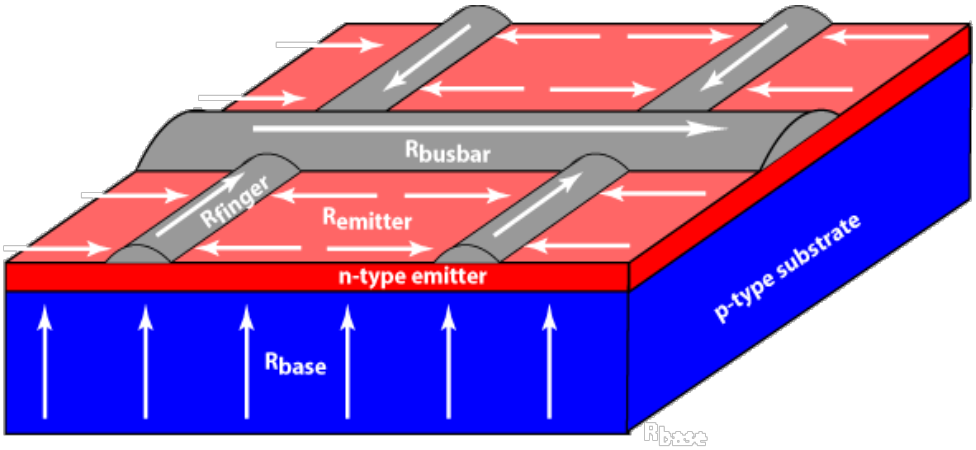

Figure 20: Resistive Components And Current Flows in a Solar Cell [37]

The total series resistance of a solar cell is due to the contributions from the following [37] (as illustrated in figure 20):

1. Resistance due to the base (R_{base})
2. Resistance due to the emitter ($R_{emitter}$)
3. Resistance due to busbars (R_{busbar})
4. Resistance due to fingers (R_{finger})
5. Resistance due to contact of metal with the emitter (R_c)

The series resistance results in the power loss in the cell. Furthermore, there's additional power loss owing to shading due to the front metal coverage. Expressions for power losses due to each resistance component and for shading is derived according to [38] which will be helpful in optimizing the front grid design.

A simple elementary section is considered which represents the contact grid pattern for solar cells. This section is '2nb' units wide, has 'n' number of gridlines each 'a' units long and spaced '2b' units apart. 'w' is the width of the gridlines and 'w'' is half of the width of the busbar. Expressions will be derived for the full section and then normalized to unit area by dividing them by the area '2nab'.

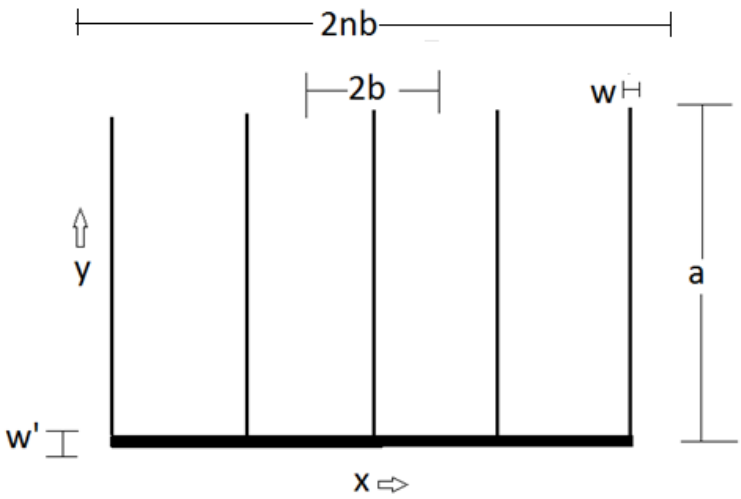

Figure 21: Elementary Contact Grid Pattern

1) Power Loss due to the Base:

   Power loss due to the current flowing through the thickness of the base as shown in the figure 20 is given simply by

$$P_{base} = I^2 R_b = 2J_L^2 nabl\rho_b \qquad 7.1.1$$

   Where ρb is the resistivity of the base and l is the thickness of the base.

2) Power loss due to emitter:

   Power loss due to the current travelling through emitter layer of the solar cell (n^+ layer in an n^+-p cell) is given by the following equations. The current in the

emitter flows in the layer in x axis towards the gridline (finger). I(x) is the current in a thin strip 'a' units long and dx wide at a position x with its resistance as dR.

$$P_{emitter} = 2n \int_0^b I^2(x)\, dR \qquad 7.1.2$$

And, $dR = R_s * dx/a,$ 7.1.3

$$I(x) = \int_x^b J_L a\, dx = J_L a(b - x) \qquad 7.1.4$$

Rs is the emitter sheet resistivity, J_L is the light generated current.

Substituting equations 7.1.3 and 7.1.4 in 7.1.2, we get,

$$P_{emitter} = (2/3)\, J_L^2 n a b^3 R_s \qquad 7.1.5$$

3) Power Loss due to Fingers (Gridlines):

The current travels along the fingers in y-axis (in the figure 21) towards the busbar. Power loss due to the current flowing through the fingers is given by

$$P_{finger} = n \int_0^a I^2(y)\, dR \qquad 7.1.6$$

And, $dR = \rho_f/(wt)\, dy,$ 7.1.7

Where ρ_f is the resistivity of the finger, *t* is the thickness of the fingers.

$$I(y) = 2\int_a^y J_L\, b(y - a) \qquad 7.1.8$$

Substituting equations 7.1.7 and 7.1.8 in 7.1.6, we get,

$$P_{finger} = (4/3)\, J_L^2 n a^3 b^2\, \rho_f\, /(wt) \qquad 7.1.9$$

4) Power Loss due to Busbars:

The current from the gridlines is collected in the busbar and flows along the busbar. It is assumed that the current enters the busbar continuously, not in discrete steps. Power loss due to current flowing through the busbar is given by

$$P_{busbar} = 2\int_0^{nb} I^2(x)\, dR_b \qquad 7.1.10$$

And, $dR = \rho_f/(w't)\, dx$ 7.1.11

$$I(x) = \int_{nb}^{x} J_L\, a\, dx = J_L a(x - nb) \qquad 7.1.12$$

Substituting equations 7.1.11 and 7.1.12 in 7.1.10, we get,

$$P_{busbar} = (2/3) J_L^2 n^3 a^2 b^3\, \rho_f/(w't) \qquad 7.1.13$$

5) Power Loss due to Contact Resistance:

There is power loss due to the metal gridlines and busbars making contact with the emitter after undergoing firing.

$$P_{contact} = 2nI^2 R_c \qquad 7.1.14$$

And, $I = J_L a\, b$ 7.1.15

$$R_c = (\rho_c R_s)^{1/2}/a \qquad 7.1.16$$

Substituting equations 7.1.15 and 7.1.16in 7.1.14, we get,

$$P_{contact} = 2J_L^2(\rho_c R_s)^{1/2} n a b^2 \quad 7.1.17$$

The total power loss due to various components of resistance in a solar cell is,

$$P_{resistance} = P_{base} + P_{emitter} + P_{finger} + P_{busbar} + P_{contact} \quad 7.1.18$$

The total resistance of the solar cell is given by,

$$r_s = P_{resistance} / J_L^2 \quad 7.1.19$$

The resistance expressions obtained from the power loss normalized to unit area of the cell (obtained by dividing each expression by 2nab) are given as following in the table 2:

Table 2: Expressions for the Resistance Components of the Solar Cell

Resistance component	Expression (Ω-cm²)
R_{base}	$\rho_b l$
$R_{emitter}$	$(1/3)\, b^2 R_s$
R_{busbar}	$(1/3)\, n^2 a b^2 \ \rho_f /(w't)$
R_{finger}	$(2/3)\, a^2 b \ \rho_f /(wt)$
$R_{contact}$	$b(\rho_c R_s)^{1/2}$

There is power loss due front metal grid shading which is given by,

$$P_{shading} = P_L n\eta[aw+2bw'] \quad 7.1.20$$

The total power loss in the cell is given by:

$$P_{total} = P_{resistance} + P_{shading} \quad 7.1.21$$

7.2 Modifications to the Model

The pattern of the model for calculating the series resistance of a solar cell discussed earlier is called the H-type grid pattern. It is based on some assumptions and represents the ideal case scenario. However, to accurately predict the series resistance and to use the model to optimally design the front grid metallization pattern, it is important to modify the model in order to incorporate non-idealities. In this section, some of the assumptions of the H-type model will be discussed followed by the modifications that will lead to new models (as discussed and derived in [39]) which can be used to better emulate the practical scenario.

Given below are few assumptions in the H-type grid pattern (or rectangular) model [39]:

1) The gridlines have a rectangular cross-section.
2) The fingers are uniform.
3) The fingers are wider than at least 1.5 times the transfer length of the contact.
4) The current from the fingers enters the busbar continuously and not in discrete quantity.

5) The flow of light generated current is uniform from the base to the emitter, after which it laterally spreads to the fingers.
6) The illumination on the solar cell is uniform.

7.2.1 Non Ideal Finger Shape

Practically, the screen-printed fingers do not have ideal rectangular shape. Evident from the SEM images of the cross section of the fingers as shown in figures 22 & 24, it is possible to approximate the cross-section area of a practical screen-printed solar cell finger by Gaussian or Trapezoidal shape.

i. Gaussian Model

The following SEM images of the cross-sectional area of the fingers show that they have a bell curve shape. Thus the Gaussian function can be used since its graph has the symmetric bell curve shape.

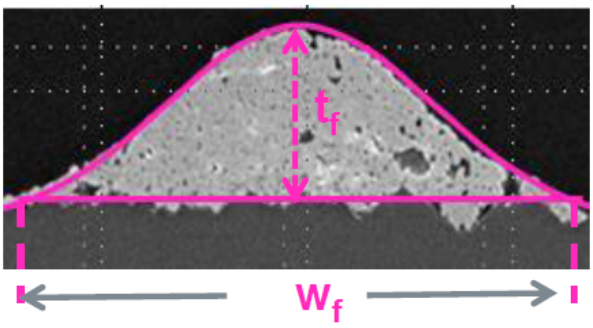

Figure 22: Screen-printing Grid Finger Cross-Section Area- Gaussian Shape [39]

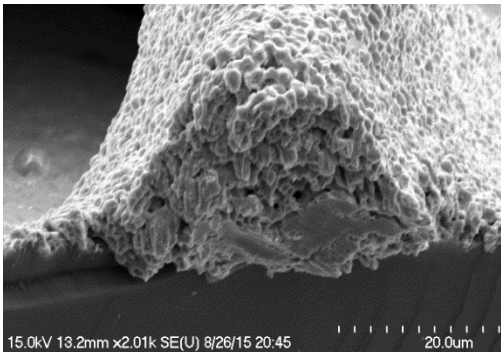

Figure 23: Gaussian Shape Cross-Section Area of Grid Finger Screen-Printed at SPL

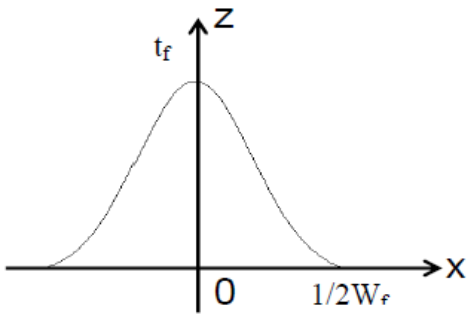

Figure 24: Gaussian Profile of a Grid Finger

The gaussian function has the form as shown below [40]:

$$f(x) = a \exp\left(-\frac{(x-b)^2}{2c^2}\right) \qquad 7.2.1$$

The area under the curve given by:

$$\int_{-\infty}^{\infty} ae - \frac{(x-b)^2}{2c^2} dx = ac\sqrt{2\pi} \qquad 7.2.2$$

And the parameter c related to the full width at half maximum (FWHM) of the peak according to $\text{FWHM}=2\sqrt{2ln2}\,c$ 7.2.3

Where *a* is the peak height of the curve, *b* is the center position of the peak and *c* is the standard deviation.

Thus, for the cross-sectional profile of the finger as shown in figure 22 the function can be written as:

$$f(x) = t_f e^{-\frac{x^2}{2\sigma^2}} \quad 7.2.4$$

Where t_f is the peak height of finger, w_f is the width of the finger and σ is the standarrd deviation.

The area of the profile *A* is given by :

$$A = \int_{-\infty}^{+\infty} f(x)dx = t_f \sigma \sqrt{2\pi} \quad 7.2.5$$

$$And,\ FWHM = 2\sqrt{2ln2}\ \sigma \quad 7.2.6$$

According to [39], $s = FWHM / w_f$ 7.2.7

and so area $A = \frac{sw_f t_f \sqrt{\pi}}{2\sqrt{ln2}}$ 7.2.8

We know that, $dR = (p_f / A)dy$, 7.2.9

thus, $dR = \frac{p_f 2\sqrt{ln2}}{sw_f t_f \sqrt{\pi}} dy$ 7.2.10

Substituting 7.2.10 and 7.1.8 in 7.1.9, we get, $P_{finger} = (8/3) J_L^2 n a^3 b^2 \rho_f \frac{\sqrt{ln2}}{sw_f t_f \sqrt{\pi}}$ *7.2.11*

ii. Trapezoidal Model

In cases like that of double printing (which will be discussed later), it can be observed that the cross-section of the finger can have the shape like that of a trapezoid as shown in figure 25.

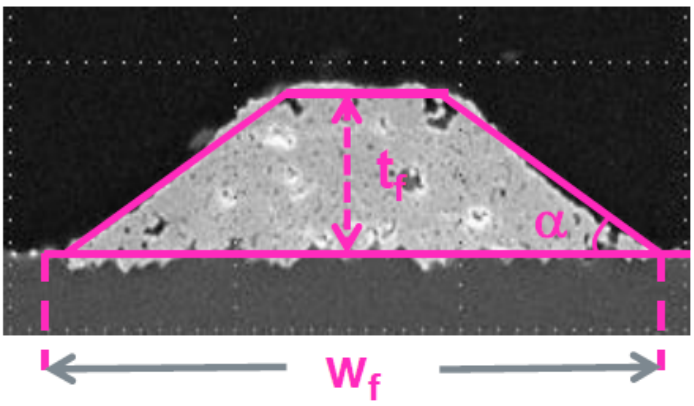

Figure 25: Screen-printing Grid Finger Cross-Section Area- Trapezoid Shape [39]

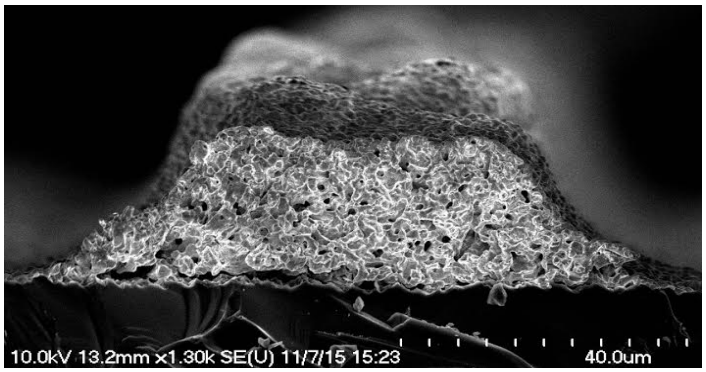

Figure 26: Trapezoidal Shape Cross-Section Area of Grid Finger Screen-printed at SPL

The cross sectional area of the trapezoidal shape with the finger width w_f, finger height t_f and the side wall of the finger making α degrees from the horizontal (its slope is tan α) can be given by:

$$A = w_f t_f - \frac{t_f^2}{tan\alpha} = (w_f - \frac{t_f}{tan\alpha})\, t_f \qquad 7.2.12$$

Substituting 7.1.12 in 7.2.9, we get $$dR = \frac{\rho_f}{(w_f - \frac{t_f}{tan\alpha})\, t_f} dy \qquad 7.2.13$$

Substituting 7.1.13 in 7.1.9, $$P_{finger} = (4/3) J_L^2 n a^3 b^2 \frac{\rho_f}{(w_f - \frac{t_f}{tan\alpha})\, t_f} \qquad 7.2.14$$

7.2.2 Non Uniformity of Fingers

The screen-printed fingers practically aren't perfectly uniform as opposed to the smooth and uniform fingers assumed in the rectangular model. This is one of the reasons that causes the discrepancy between the ideal resistance calculated and the measured series resistance of the solar cells.

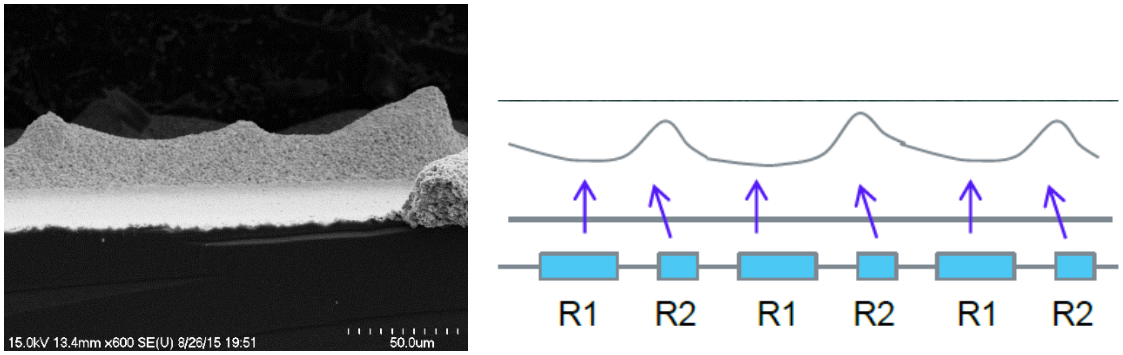

(a) (b)

Figure 27: (a) SEM Image Depicting Non-Uniform Fingers (b) Pictorial Representation of Incorporating Non-Uniformity in the Model [39]

As seen from the side view of the finger of a screen-printed solar cell (figure 27(a)) shown above, the surface of the fingers are not smooth, but consist of imperfections in the form of rough surface. These 'peaks' and 'valleys' seen in the figure are caused by the

wire mesh of the screens and hence are relatively consistent or regular over the length of the fingers. Lin Jiang *et al.* in [39] have introduced a term called "roughness coefficient" 'f' which is given by: $f = \frac{R_2}{R_1}$, where R_2 represents the resistance of the peak area and R_1, of the valley area.

Total resistance of the finger (with uneven surface) = $R_{non-uniform} = R_1+R_2 + R_1+R_2 \ldots = \mathrm{M}(1+f)R_1$

If the surface was even and uniform then the resistance would have been $R_{uniform} = R_1+R_1 + \cdots = 2\mathrm{M}R_1$

Thus, $R_{non-uniform} = \frac{(1+f)}{2} R_{uniform}$ 7.2.15

The power loss expressions *7.1.11* and 7.1.14 will be modified to the following expressions to include the effect of surface roughness:

(Gaussian model) $P_{finger} = (8/3)\, J_L^2 n a^3 b^2\, \rho_f \frac{(1+f)\sqrt{ln2}}{s w_f t_f \sqrt{\pi}}$ 7.2.16

(Trapezoidal model) $P_{finger} = (4/3)\, J_L^2 n a^3 b^2 \frac{\rho_f (1+f)}{(w_f - \frac{t_f}{tan\alpha})\, t_f}$ 7.2.17

7.2.3 Contact Resistance

The contact resistance expression in the rectangular grid model assumes that the width of the fingers is at least 1.5 times larger than the transfer length as for $\frac{w_f}{2} >$, *coth*

$(\frac{w_f}{2L_T}) \cong 1$. However, if the trend of reducing the finger widths is followed, the assumption loses its validity. The contact resistance expression becomes:

$$R_c = \frac{L_T R_S}{a} coth\ (\frac{w_f}{2L_T}) \qquad 7.2.18$$

Where $L_T = \left(\frac{\rho_c}{R_c}\right)^{\frac{1}{2}}$ 7.2.19

Thus the expression of power loss due to contact resistance is given by:

$$P_{contact} = 2J_L^2(\rho_c R_s)^{1/2} na\, b^2\ coth\ (\frac{w_f}{2}\sqrt{\frac{R_s}{\rho_c}}) \qquad 7.2.20$$

7.2.4 Current Entering Bus Bars

In the rectangular H-type model, it is assumed that the current from the fingers enters busbar along its length continuously. However, in reality, the current enters the busbars in discrete quantity. The current from a finger enters the busbar and flows along it until the current from the next finger is added to the existing current and they flow along the busbar and so on. Applying this modification [41], the new expression for the power loss is: $P_{busbar} = (2/3)J_L^2 n(n+1)(n+2)a^2 b^3\, \rho_f\, /(w't)$

8. OPTIMUM FINGER SPACING

8.1 Optimization

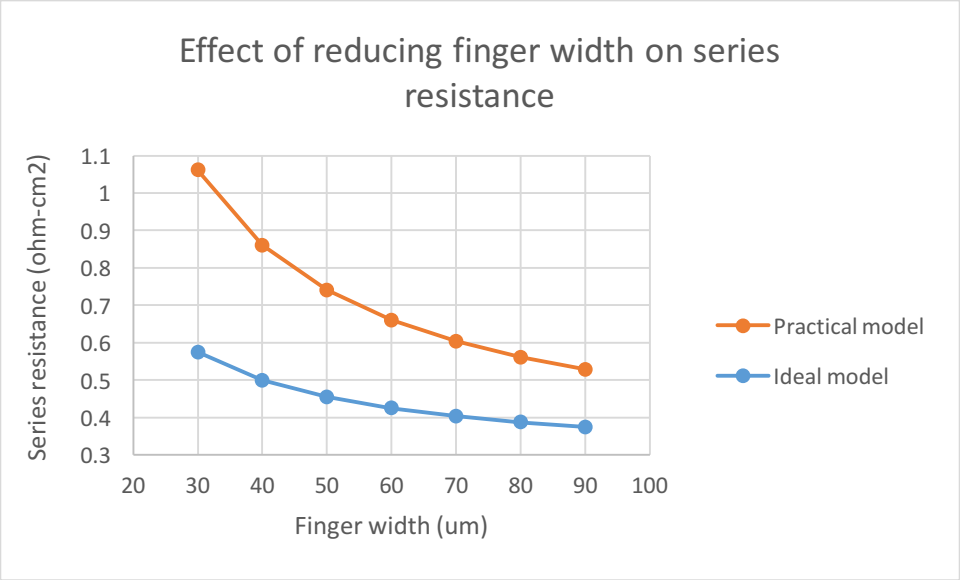

Figure 28: Graph Showing the Effect of Reducing Finger Width on Series Resistance

As seen from the graph above, the series resistance, for a given finger spacing, increases with reducing finger width, and, the increase much more prominent in practical case scenario as compared to the ideal case scenario. For the above shown graph H-type rectangular grid pattern is used to model the ideal case scenario and for the practical case scenario all the modifications discussed in the previous chapter (with the Gaussian model for fingers) is incorporated.

However, the front metal coverage is reduced as the finger width reduces, and hence the shading loss decreases. Therefore, there is a need to find optimal finger spacing to achieve the optimal front metal coverage that can keep both the shading losses as well as series resistance losses of the cell as low as possible. This is done by running a

MATLAB code to minimize the total power loss, $P_{total} = P_{resistance} + P_{shading}$ for a specific finger width by keeping it constant and varying the finger spacing over a practical range of values. The optimum finger spacing is found where the sum of $P_{resistance}$ and $P_{shading}$ curves is the minimum, i.e. where the P_{total} curve has the minima as shown in the figure 29 below as an example, which was obtained by running the MATLAB code for finding the optimum finger spacing for finger width of 90um. In this example, optimum finger spacing obtained was 2.08mm.

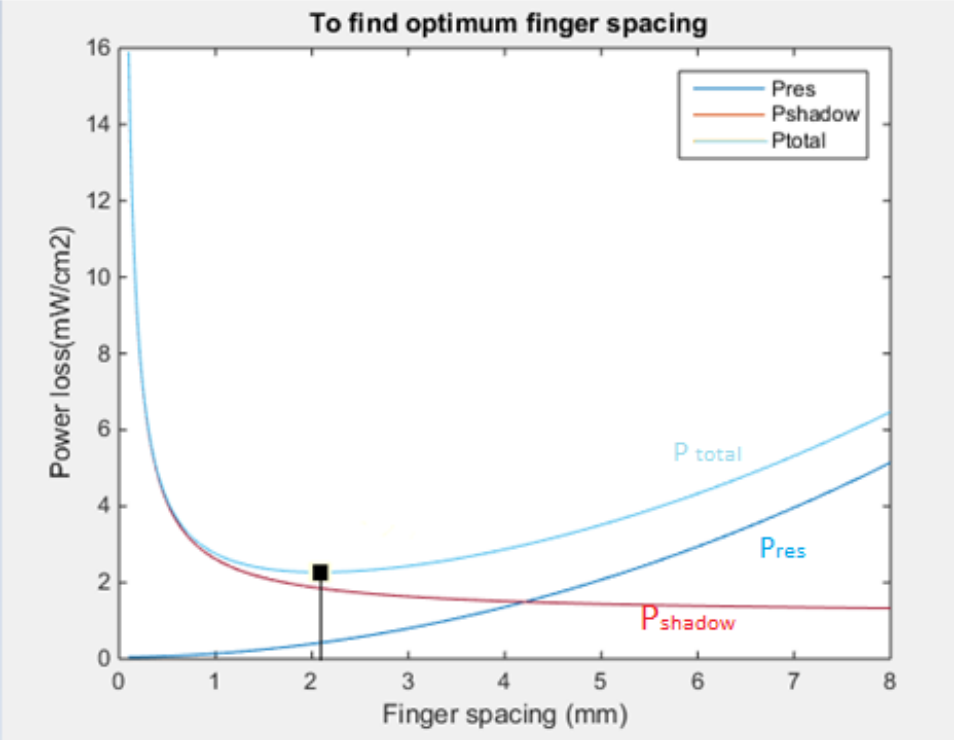

Figure 29: Output Graph of the MATLAB Code Giving the Optimum Finger Spacing for a Given Finger Width

Using this method, the screens designs with different finger widths and their corresponding optimal finger spacing were designed and the percentage of the total area

of the solar cell shaded by the front metal for each of those screens was calculated. Figure 30 shows the reduction in front metal coverage area as the finger widths is decreased.

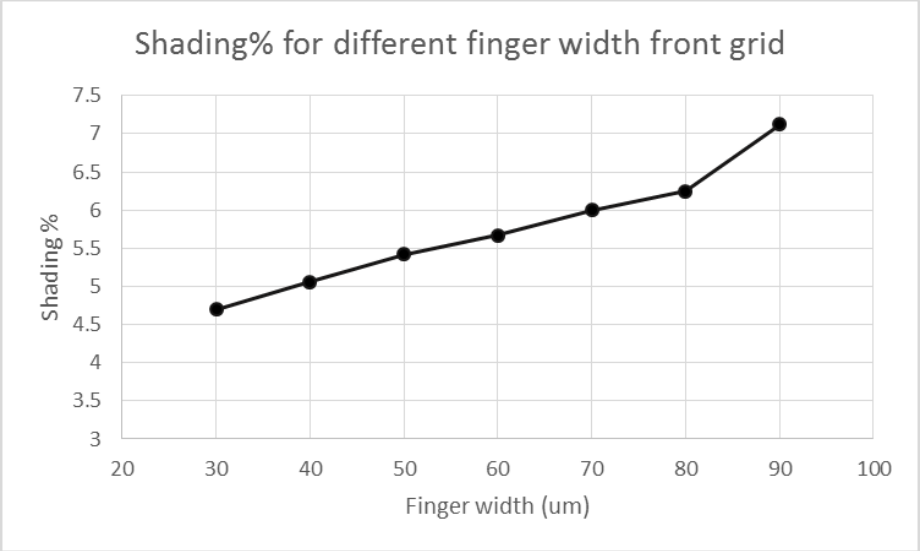

Figure 30: Graph of Percentage Shading of the Solar Cell Area for Designs with Different Finger Widths

The efforts described in this thesis to reduce the finger widths resonates with the trend in the industry towards the same as depicted in the graph shown below (figure 31) from the ITRPV Roadmap 2011. The paste manufacturers have been working towards formulating pastes that can achieve superior electrical characteristics like higher electrical conductivity and lower contact resistance for fine line printing while the screen manufacturers have been working towards advancements in the screen technology to enable fine line printing and increasing the aspect ratio [36]. It is predicted that by 2020, in the industry, the line width used would be reduced to approximately a quarter from that in 2010 (from 100um to around 25-30um).

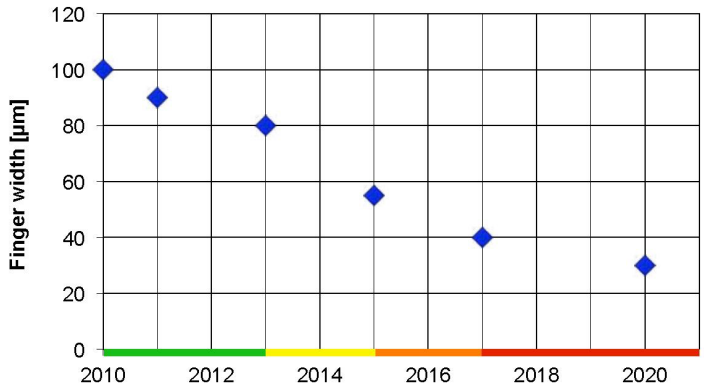

Figure 31: Predicted Trend of Finger Width [36]

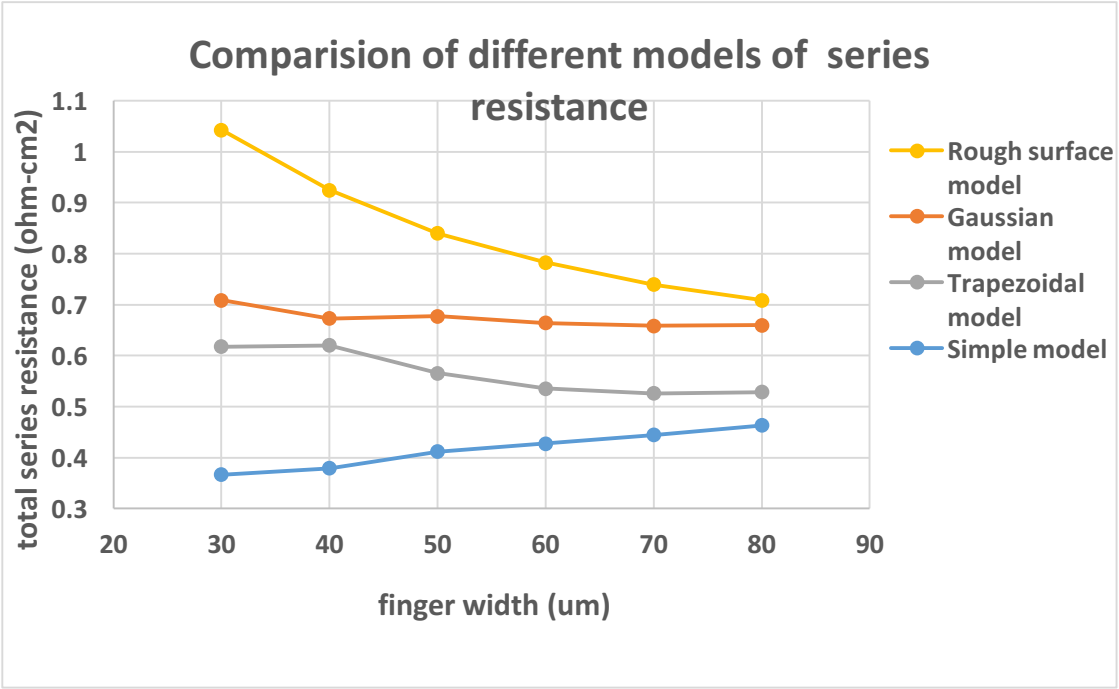

Figure 32: Graph Showing Comparison of Different Models of Calculating Series Resistance

The graph shown in figure 32 shows comparison of different models of calculating series resistance which are calculated for single printed solar cells with three busbars.

8.2 Results from the Griddler Simulation Model

The various parameters of the solar cell obtained from the baseline solar cell results along with the new reduced finger widths and their corresponding finger spacing are given as input to a simulation program called Griddler. “Griddler is a finite element model (FEM) simulation program developed at the Solar Energy Research Institute of Singapore (SERIS). It solves the voltage and current distributions in the cell planes at arbitrary illumination and biasing conditions” [42]. The electrical parameters obtained from the output of the Griddler simulations are listed in the table 3. It is seen that as the finger width is reduced, there is improvement in efficiency. There is an absolute overall efficiency gain of 0.43% for the grid with reduced finger width as compared to the baseline cells.

Table 3: Results of Griddler Simulation

Finger width (um)	Voc(mV)	Jsc (mA/cm2)	FF(%)	Efficiency(%)
90 (Baseline)	616	35.57	78.71	17.24
80	616	35.90	78.45	17.36
70	617	36.00	78.53	17.43
60	617	36.13	78.52	17.5
50	617	36.22	78.60	17.57
40	617	36.36	78.55	17.62
30	617	36.50	78.55	17.67

9. EXPERIMENTAL WORK

9.1 Screen Layout

The screens using the optimized design calculations are designed using the DW2000 software from Design Workshop Technologies Inc. Double printing requires high alignment accuracy to ensure print of second layer of pastes accurately on the top of the first layer. Thus, small circular fiducials are used as alignment targets. There are two outboard fiducials for the mask alignment. These are filled with epoxy to give the fiducials a good contrast from the background. Three inboard fiducials (without epoxy) are used for wafer alignment as shown in the figure 33.

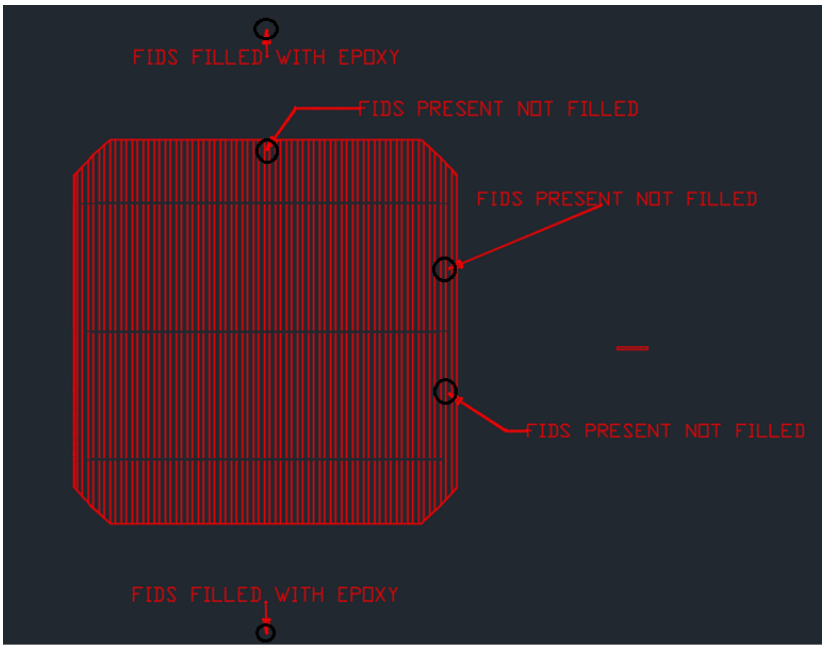

Figure 33: Screen Layout for the Screen with Locations of Fiducials Circled in Black

9.2 Setting Up the Double Printing Program in the Baccini Printer

Two different programs are used for printing the first and second layers. Let us call them Print-1 and Print-2 programs respectively. The following procedure is for the initial set up:

1. Input and then adjust the location coordinates for the camera sensors to locate the outboard fiducials for mask alignment for both the programs.
2. For the Print-2 program, additionally, input and then adjust the location coordinates for the camera sensors to locate the printed fiducials on the wafer for accurate alignment of wafer for the second print.
3. 'Train' the program to identify the fiducials as a 'circle' and adjust its size.
4. Adjust and set the contrast and threshold limits for the camera to differentiate fiducial/fiducial print from the background.

9.3 Testing of the Best Paste Configuration

Two experimental pastes were received from Heraeus, paste A and paste B. There was a need to test out the paste sequence for double printing to find out which sequence works best for the cells fabricated in SPL. Trial runs were made by printing cells with finger width 80um in all four possible paste layer sequences: A-A, A-B, B-A, and B-B. Paste A showed good paste flooding when used for printing whereas paste was viscous and drying issues resulting in bad flooding (figures 34 & 35).The results of the testing is shown in the table below:

Table 4: Determining the Best Paste Sequence

Paste sequence	Efficiency (%)	Jsc (mA/cm²)
A-A	17.5	35.7
A-B	17.3	35.2
B-A	17.0	35.5
B-B	17.6	36.0

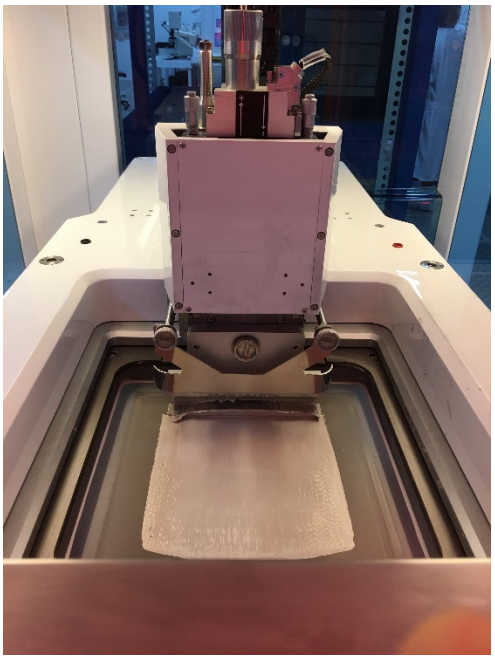

Figure 34: Good Flooding of Paste

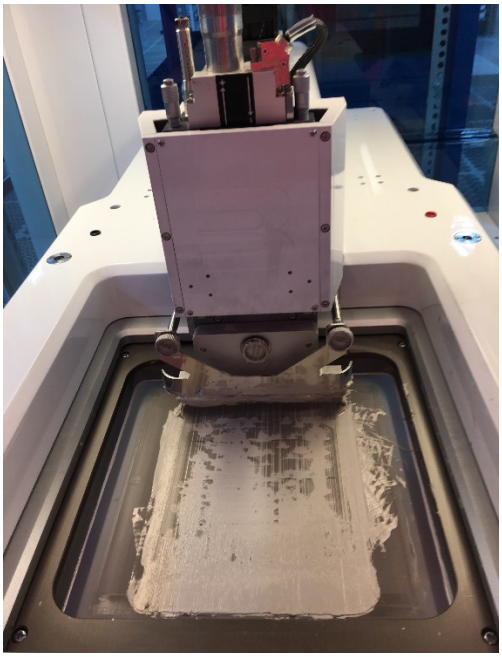

Figure 35: Bad Flooding of Paste

The sample size of the data shown was small due to the experimental paste quantity restriction. There is no clear winner but from the efficiency and the repeatability observed, B-B paste sequence was chosen to be used for all the further experimental work.

9.4 Single and Double Printing of Solar Cells

Single printing and double printing of the cells with finger widths 80um, 70um, 60um and 50um was carried out using the paste B. The efficiency, short circuit current and resistance results are shown below in figures below:

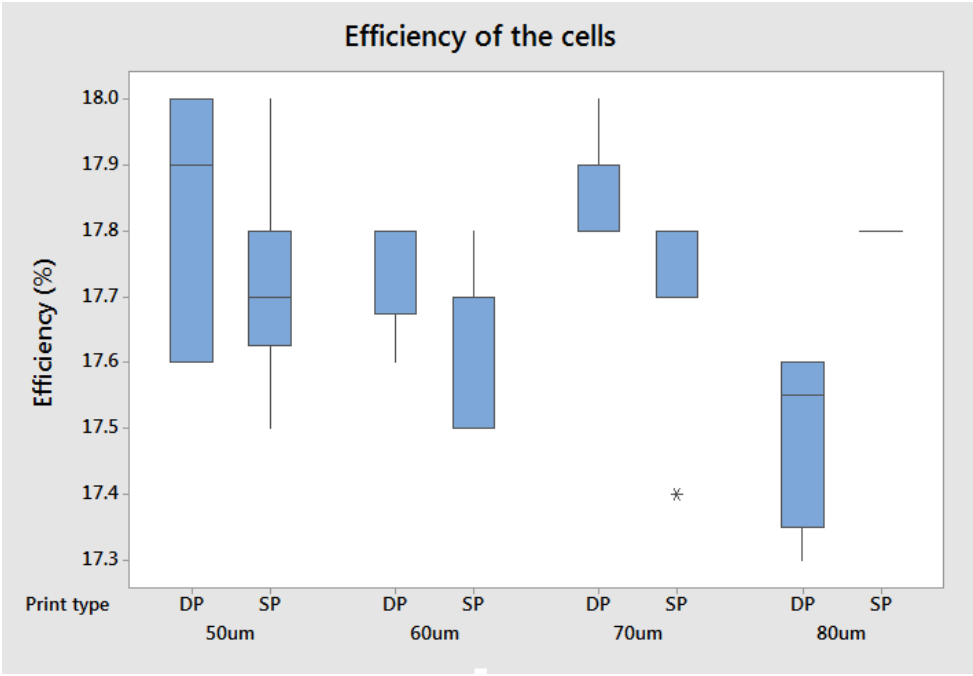

Figure 36: Boxplot Graph for Efficiency of Solar Cells

Table 5: Average Values of Efficiency of the Cells

Finger width (um)	Double printing efficiency (%)	Single printing efficiency (%)
70	17.86	17.71
60	17.75	17.64
50	17.83	17.71

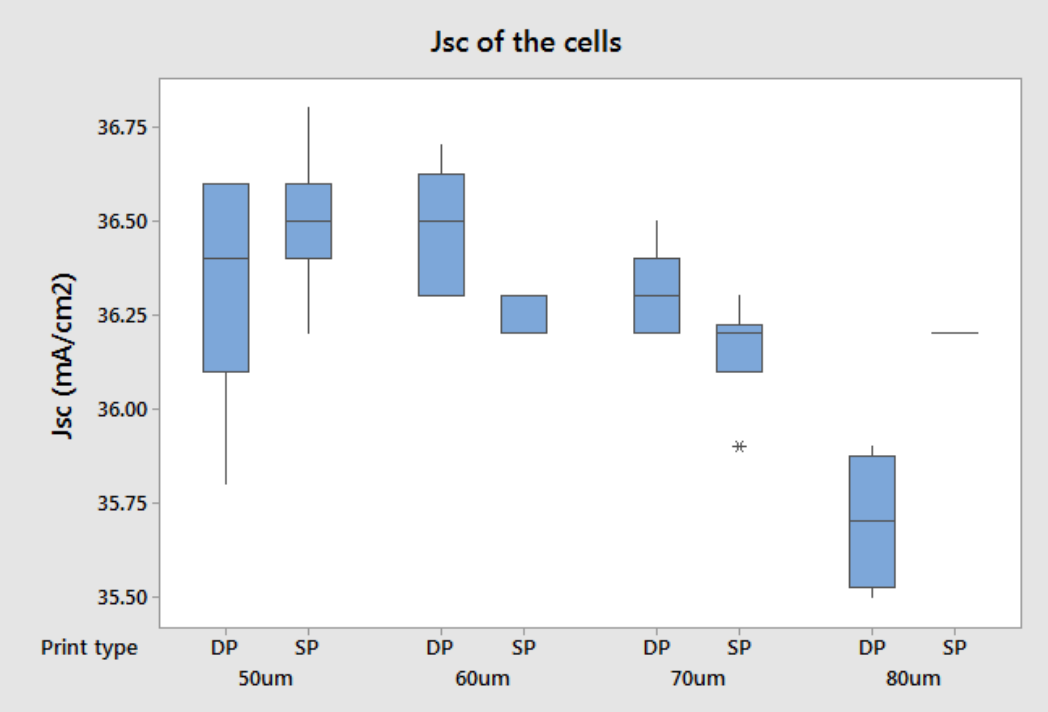

Figure 37: Boxplot Graph for Jsc of Solar Cells

Table 6: Aspect Ratios for Cells

Print type	Finger width (um)	Aspect ratio
SP	90	0.20
SP	50	0.39
DP	50	0.45

There seems to be an improvement in efficiency of double printed cells as compared to single printed cells. Similarly, the short circuit current and the aspect ratio is seen to improve with narrower finger widths. It should, however, be noted that even though there is a trend, the result is largely inconclusive and more data is needed so that the results are statistically significant. From table 5 it is observed that, improvement in efficiency for cells from single print to double print is around 0.12-0.15%, which is in good agreement with the values found in the literature [31,33]. Figure 38 shows the variation of series resistance of both the single and double printed cells as a function of their finger widths.

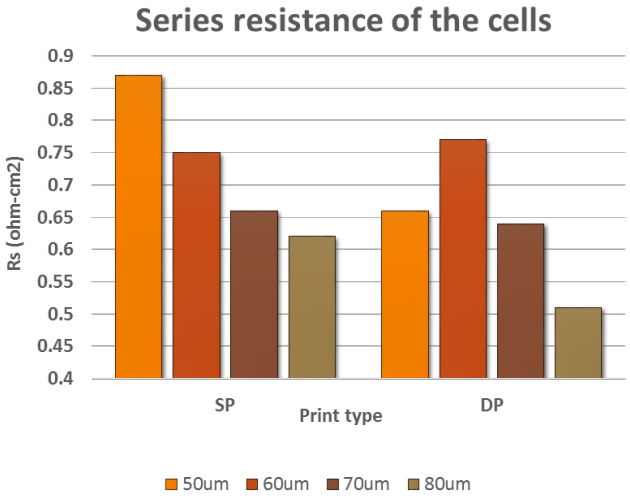

Figure 38: Graph of Series Resistance of Solar Cells

The expected increase in series resistance of the cells with decrease in their finger widths is clearly seen in figure 38. In addition, the double printed cells have lower series resistance as compared to single printed cell as evident from the figure. However, double printed lot with 60um finger width does not fit in the trend seen for rest of the lots. The reason for higher than expected series resistance for this lot is bad printing of the lot causing finger interruptions and broken fingers. This is seen from the poor electroluminescence image of the cells (figure 40) and verified when the fingers are examined under the microscope (figure 39).

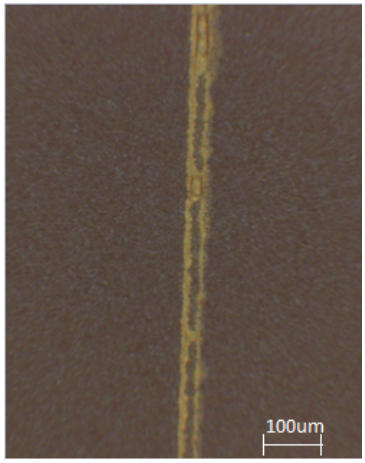

Figure 39: Finger Interruptions

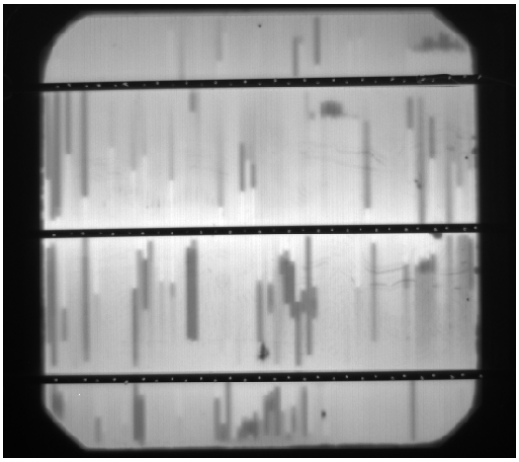

Figure 40: EL Image of the Double Printed 60μm

9.5 Factors Bringing Down the Efficiency of the Cells

There are a few problems associated with using wire mesh screens for printing. Some of them are as follows:

1) Paste bleeding (Fig. 41 (a))
2) Gridline interruption for narrow finger width design (Fig.41 (b))
3) Mesh marks making surface rough (Fig.41 (c))
4) Screens getting clogged easily

All these result in lower Jsc and higher fill factor, thereby causing reduction in the efficiency.

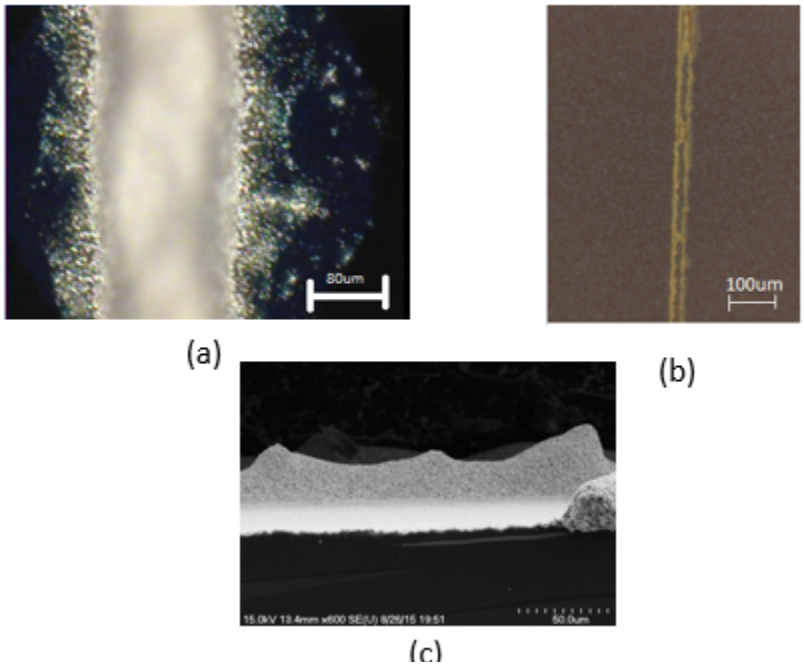

Figure 41: Problems with Mesh Screen-printed Fingers

10. FUTURE WORK

Based on the observations of the results of the experiments, a few key things were identified which could help with further improvements:

1) Switch to stencils for narrower finger widths- Dual printing with stencils to have higher aspect ratio and further improvements in Jsc. The problems with using mesh screens described in the previous section can be overcome by using stencils. Stencil use can result in smooth finger profile in combination with high aspect ratio, excellent paste transfer efficiency and line height uniformity. Even with lower height the fingers will be highly conductive because of nearly flat surface profile along finger length (figure 42)

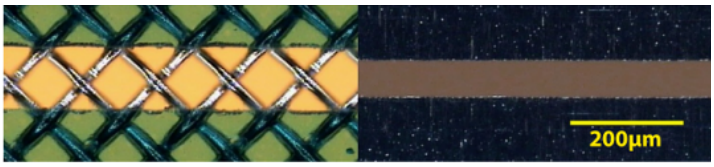

Figure 42: Stencils Have 100% Open Aperture and Provide Fine Lines with High Aspect Ratio [43]

2) Improve alignment accuracy- High alignment accuracy is very important for print-on-print method, especially in the industry, for high repeatability and ensuring high throughput rates. The alignment accuracy of the prints can be further improved by modifying the current screen design to include 4 fiducials (2 on right and 2 on left side of the wafer as shown in the figure 43)

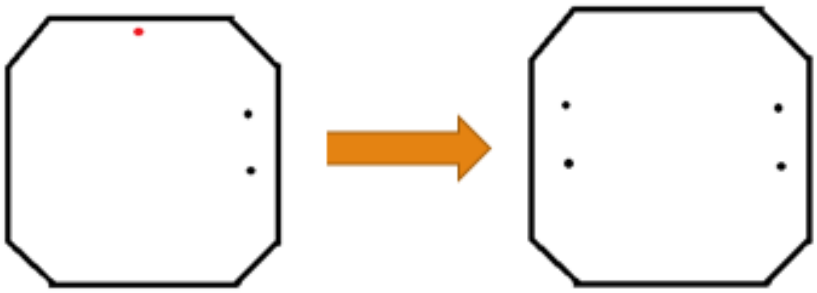

Figure 43: Changing the Location and Number of Fiducials for Accurate Alignment

3) Ag Pastes- The process for double printing is already developed. There is a need to get non-firing paste for second layer and better pastes in general that work well for the cells fabricate din SPL, and perform subsequent design of experiments (DOE) of the pastes.
4) Better emitter - Current emitter is very heavily doped and might be limiting the performance of the cell. If the doping level is reduced to improve the emitter, it will cause an increase in the sheet resistance and it would become increasingly difficult to contact the emitter. In this case, the double printing method would prove to be very helpful due to the differentiated pastes for different layer which enables us to have the first layer optimized to contact the emitter. This would potentially lead to significant gain in efficiency.

11. CONCLUSION

In this thesis, optimization of the front grid metallization for the diffused junction solar cells fabricated in Solar Power Laboratory was achieved resulting in the overall efficiency gain of 0.6% for the solar cells. This was done by targeting the shading losses and reducing the front metal coverage to improve the short circuit current. The basic model of series resistance was expanded to include the modifications to capture the effects of screen-printing. Incorporating those effects, series resistance for grid with narrow finger widths were predicted and then the finger spacing was optimized for each of the chosen finger widths to balance the shading and resistance losses and minimize the total loss. In addition, the process for double printing was developed with good alignment accuracy for finger width down to 50um. Improvement in efficiency was demonstrated with the average efficiency of the cells increasing from 17.2% to 17.8%, with peak efficiency of 18%.

12. REFERENCES

[1] Mitigation, Climate Change. "IPCC special report on renewable energy sources and climate change mitigation." (2011).

[2] “Leading scientists: energy crisis poses major 21st century threat, action needed now” (biopact). [Online]. Available: http://news.mongabay.com/bioenergy/2007/10/leading-scientists-energy-crisis-poses.html

[3] Energy and Climate Change, World Energy Outlook Special Report, International Energy Agency

[4] Realizing a Clean Energy Future: Highlights of NREL Analysis (Brochure)

[5] 2013 Renewable Energy Data Book, National Renewable Energy Laboratory (NREL).

[6] Nemet, Gregory F, "Beyond the learning curve: factors influencing cost reductions in photovoltaics." Energy policy 34.17 (2006): 3218-3232.

[7] SunShot, U.S. Department of Energy (DOE), “Photovoltaic System Pricing Trends: Historical, Recent, and Near-Term Projections (2014 Edition),” [Online]. Available: http://www.nrel.gov/docs/fy14osti/62558.pdf

[8] Case study of a growth driver – silver use in solar (Case study of a growth driver – silver use in solar) [Online]. Available: http://www.pvtech.org/guest_blog/case_study_of_a_growth_driver_silver_use_in_solar

[9] Michael Puttre, “Future Solar Cost Reductions Hinge on Raising Solar Cell Efficiencies,” [Online]. Available: http://www.solarindustrymag.com/issues/SI1410/FEAT_01_Future-Solar-Cost-Reductions-Hinge-On-Raising-Solar-Cell-Efficiencies.html

[10] Hannebauer, Helge, Thorsten Dullweber, Tom Falcon, Xiao Chen, and Rolf Brendel. "Record Low Ag Paste Consumption of 67.7 Mg with Dual Print." *Energy Procedia*: 66-71.

[11] Hannebauer, Helge, Thorsten Dullweber, Tom Falcon, and Rolf Brendel. "Fineline Printing Options for High Efficiencies and Low Ag Paste Consumption." *Energy Procedia*: 725-31.

[12] Hannebauer, Schimanke, T. Falcon, Altermatt, and T. Dullweber. "Optimized Stencil Print for Low Ag Paste Consumption and High Conversion Efficiencies." *Energy Procedia*: 67,108-15.

[13] CRC Handbook of Chemistry and Physics, 91st ed.; CRC Press: Boca Raton, FL, 2010.

[14] PVMagazine, "Natcore swaps silver for aluminum in solar cells," [Online]. Available: http://www.pv-magazine.com/news/details/beitrag/natcore-swaps-silver-for-aluminum-in-solar-cells_100020645/#ixzz3l4ytvsef

[15] Karpowich, Lindsey, Kristin Murphy, and Weiming Zhang. "Advancements in Low-silver Metallization Paste for Si Solar Cells." *2012 38th IEEE Photovoltaic Specialists Conference*.

[16] Saga, Tatsuo. "Advances in Crystalline Silicon Solar Cell Technology for Industrial Mass Production." *NPG Asia Materials*: 2, 96-102. Retrieved from http://www.nature.com/am/journal/v2/n3/full/am201082a.html

[17] ISFH, "19.6% Efficient Large Area Fully Screen-printed Silicon Solar Cells," [Online]. Available: http://www.isfh.de/institut_solarforschung/industrienahe-siebdrucksolarzelle.php?_l=1.

[18] Restrepo, and Backus. "On Black Solar Cells or the Tetrahedral Texturing of a Silicon Surface." *IEEE Trans. Electron Devices IEEE Transactions on Electron Devices*: 1195-197.

[19] C. Honsberg and S. Bowden, "PVCDROM," [Online]. Available: http://www.pveducation.org/pvcdrom/properties-of-sunlight/atmospheric-effects.

[20] S. Herasimenka, Process PhD Comprehensive Exam: Development for 20% Silicon Heterojunction Solar (SHJ) Cell and Analysis of Loss Mechanisms, Tempe, 2013.

[21] D. Kumar, S. Saravanan and P. Suratkar, "Effect of Oxygen Ambient During Phosphorous Diffusion on Silicon Solar Cell," *Journal of Renewable and Sustainable Energy*, no. 4, p. 033105, 2012.

[22] J. Nelson, "7.4.5 Strategies to Reduce Surface Recombination," in The Physics of Solar Cells, Covent Garden, Imperial College Press, 2004, pp. 191-193.

[23] C. Honsberg and S. Bowden, "PVCDROM," [Online]. Available: http://www.pveducation.org/pvcdrom/solar-cell-operation/quantum-efficiency

[24] W. Shockley and H. 1. Queisser, "Detailed Balance Limit of Efficiency of p-n Junction Solar Cells," *Journal of Applied Physics*, vol. 32, no. 3, pp. 510-519, 1961.

[25] R. M. Swanson, "Approaching the 29% limit efficiency of silicon solar cells," Proc. of the 31" *IEEE PVSC*, 2005, pp. 889-894.

[26] Solanki, C. S, Solar Photovoltaics: Fundamentals, Technologies and Applications, pp. 101-102.

[27] C. Honsberg and S. Bowden, "PVCDROM," [Online]. Available: http://pveducation.org/pvcdrom/solar-celloperation/efficiency

[28] Rose, R. De, P. Magnone, M. Zanuccoli, E. Sangiorgi, and C. Fiegna. "Loss Analysis of Silicon Solar Cells by Means of Numerical Device Simulation." *2013 14th International Conference on Ultimate Integration on Silicon (ULIS)*.

[29] A. Mette, PhD thesis, "New Concepts for Front Side Metallization of Industrial Silicon Solar Cells," University of Freigburg

[30] Ju, Minkyu, Youn-Jung Lee, Jonghwan Lee, Bonggi Kim, Kyungyul Ryu, Kyuho Choi, Kyuwan Song, Kyungsoo Lee, Changsoon Han, Youngmi Jo, and Junsin Yi. "Double Screen-printed Metallization of Crystalline Silicon Solar Cells as Low as 30μm Metal Line Width for Mass Production." *Solar Energy Materials and Solar Cells*: 204-08.

[31] M. Galiazzo, "Reliable Double Printing of Ag Contacts for c-Si Cell Manufacturing." *2010 Secondmetal Workshop Konstantz*

[32] Hannebauer, Helge, Tom Falcon, Rene Hesse, Thorsten Dullweber, and Rolf Brendel. 2011. "18.9 %-EFFICIENT SCREEN-PRINTED SOLAR CELLS APPLYING A PRINT-ON-PRINT PROCESS." *26th European Photovoltaic Solar Energy Conference and Exhibition*, 1607–10

[33] M. Galiazzo, Furin, Tonini, Cellere, & Baccini, (2010). "Double Printing of Front Contact Ag in c-Si Solar Cells." *25th European Photovoltaic Solar Energy Conference and Exhibition / 5th World Conference on Photovoltaic Energy Conversion*, 6-10.

[34] Popischil, Kuchler, Klawitter, Rodriguez, Padilla, Efinger, Biro, D. (2014). "Ultrafine front side metallization on silicon solar cells by industrial dispensing technology." *29th European Photovoltaic Solar Energy Conference and Exhibition*, 1304–1306.

[35] Y. Tsunomura, Y. Yoshimine, M. Taguchi, T. Baba, T. Kinoshita, H. Kanno, H. Sakata, E. Maruyama, and M. Tanaka, "Twenty-two percent efficiency HIT solar cell," Sol. Energy Mater. Sol. Cells, vol. 93, no. 6–7, pp. 670–673, 2009.

[36] Falcon, Clasper, (2011). "Ultra Fine Line Print Process Development for Silicon Solar Cell Metalisation." *IEEE Conference Publications*, pp.1–5.

[37] C. Honsberg and S. Bowden, "PVCDROM," [Online]. Available: http://pveducation.org/pvcdrom/design/series-resistance

[38] Meier, Schroder, (1984). “Contact resistance : its measurement and relative importance to power loss in a solar cell.” *IEEE Transactions on Electron Devices*, ED-31(5), 647–653.

[39] Jiang, L., Zhang, W., Guo, T., Kapp, D., Yan, L., & Wang, L. (2013). “An improved mathematical modeling to simulate metallization screen pattern trend for silicon solar cell.” *IEEE Tampa*, 2641–2645.

[40] Gaussian function. Retrieved from https://en.wikipedia.org/wiki/Gaussian_function

[41] Meier, D. L., Chandrasekaran, V., Gupta, A., Yelundur, V., & Rohatgi, A. (2013). “Silver contact grid : inferred contact resistivity and cost minimization in 19 % silicon solar cells.” *IEEE Journal of Photovoltaics*, 3(1), 199–205.

[42] PV Lighthouse. Retrieved from https://www.pvlighthouse.com.au/simulation/hosted/griddler/griddler.aspx

[43] Hoornstra, Jaap. 2009. “Stencil Print Applications and Progress for Solar Cells.” *PVSEC 2009*, no. September: 989–92.